Monthly Notices
of the
ROYAL ASTRONOMICAL SOCIETY

Mon. Not. R. Astron. Soc. **411,** 2615–2627 (2011) doi:10.1111/j.1365-2966.2010.17867.x

Voids in coupled scalar field cosmology

Baojiu Li[1,2]★

[1]*DAMTP, Centre for Mathematical Sciences, University of Cambridge, Cambridge CB3 0WA*
[2]*Kavli Institute for Cosmology Cambridge, Madingley Road, Cambridge CB3 0HA*

Accepted 2010 October 14. Received 2010 October 13; in original form 2010 August 21

ABSTRACT

We study the properties of voids in two different types of coupled scalar field theories. Due to the fifth force produced by the scalar field coupling, the matter particles feel stronger attraction amongst each other and cluster more quickly than they do in the standard ΛCDM model. Consequently, voids in the coupled scalar field theories start to develop earlier and end up bigger, which is confirmed by our numerical simulations. We find that a significantly larger portion of the whole space is underdensed in the coupled scalar field theories and there are more voids whose sizes exceed given thresholds. This is more prominent in early times because at later times the underdense regions have already been evacuated in coupled scalar field theories and there is time for the ΛCDM model to catch up. The coupled scalar field theories also predict a sharper transition between voids and high-density regions. All in all, the qualitative behaviour is different not only from the ΛCDM result, but also amongst specific coupled scalar field models, making voids a potential candidate to test alternative ideas about the cosmic structure formation.

Key words: methods: numerical – cosmology: theory – dark energy – large-scale structure of Universe.

1 INTRODUCTION

One of the most active research areas in modern cosmology is about the theories involving cosmological scalar fields. As a potential candidate for dark energy (Copeland, Sami & Tsujikawa 2006), for example, a canonic scalar field could have interesting properties governed by its potential. Such quintessential (Wang et al. 2000) models are studied in-depth in the literature, seeing various potentials proposed, their properties investigated and their specific forms tried to be connected to developments in high-energy physics. Even richer phenomenology is achieved by considering variants of the simple quintessence model, such as giving the scalar field a non-canonical kinetic term (Armendariz-Picon, Mokhanov & Steinhardt 2000) or coupling it to the matter fields (Amendola 2000) or even the space–time curvature (Perrotta & Baccigalupi 1999), the latter case also covering certain modified gravity theories, such as the metric (Carroll et al. 2005) and Palatini (Vollick 2003) $f(R)$ gravity and Brans–Dicke theory (Brans & Dicke 1961). Often in these models, the behaviour of the scalar field is additionally controlled by a coupling function, and extra (fifth) forces are not uncommon. Local experiments then force the model builders to design specific mechanisms by virtue of which the (usually) severe experimental and observational constraints are not to be challenged, and remarkably these could be realized neatly by choosing appropriate scalar potential and/or coupling function, as in the chameleon (Khoury & Weltman 2004; Hu & Sawicki 2007; Li & Barrow 2007; Mota & Shaw 2007) and environment-dependent dilaton (Brax et al. 2010) models.

An interesting property of these models is that either the mass of the scalar field or its coupling strength is sensitively dependent on the environments, in such a way that the fifth force is suppressed where the observations and measurements are made. Taking the chameleon model as an example, in high-density regions the scalar field becomes very massive so that scalar field quanta could not propagate far and the fifth force gets suppressed. Exactly how massive the scalar field will be is determined by the local matter density as well as the steepness of the scalar potential and its derivatives, and the model could be so designed that the fifth force is suppressed in solar system but not on galactic and larger scales (Hu & Sawicki 2007), leaving the possibility that the structure formation process could be significantly affected.

As one wants the scalar field mass to fluctuate strongly across the space, a high degree of non-linearity is inevitable. In chameleon model this is often reflected in the fact that the scalar field potential is very non-linear, and in such circumstances linear treatment obviously fails. N-body simulations are then the natural method to be used to study structure formation in these models, and in this paper we shall apply this very technique to study the void properties of them.

Voids (van de Weygaert & Platen 2009) are an important ingredient of the standard picture of hierarchical structure formation. Because the initial matter distribution in the Universe is inhomogeneous, as time passes by the overdense regions will pull more matter

★E-mail: b.li@damtp.cam.ac.uk

towards them and underdense regions get emptied to form voids. For the ΛCDM cosmology, void phenomenon (Peebles 2001) is well studied (Tinker & Conroy 2009). In coupled scalar field models, the fifth force, if unsuppressed, will boost the clustering of matter and therefore help in the evacuation of underdense regions more quickly. A higher degree of emptiness in voids than what the concordance ΛCDM model predicts is thus an indicator of a possible fifth force (Keselman, Nusser & Peebles 2010). The voids are of even greater importance to chameleon models because, by naive expectation, the fifth force in these models is suppressed in high-density regions and shall not affect the galaxies clusters much, while in voids they are stronger and their effects are more significant. It is therefore interesting to see what distinct features the voids have in these models compared with those in ΛCDM. As a preliminary work, we shall only consider dark matter voids (Colberg et al. 2005) here, and leave the more technical work involving baryons to the future.

In this work we will investigate two coupled scalar field models, one in which the scalar field is a chameleon and the other in which the scalar field is not a chameleon. In practice, there is no sharp distinction between them. For the scalar potential described by equation (10) below, for example, the scalar field has no chameleon features if parameter $\alpha \sim \mathcal{O}(0.1-1)$, but will become a chameleon while $\alpha \ll 1$. Therefore, although for the non-chameleon models the fifth force is unsuppressed and thus could be well approximated as being proportional to gravity, as is commonly assumed by most N-body simulation works for coupled scalar field models to date (to name a few, Maccio et al. 2004; Kesden & Kamionkowski 2006; Farrar & Rosen 2007; Hellwing & Juszkiewicz 2009; Keselman, Nusser & Peebles 2009; Baldi et al. 2010), for safety we shall solve the scalar field value as a function of spatial position explicitly and then differentiate to compute the fifth force (Li & Zhao 2009, 2010a,b) [this technique has recently been applied to varying fundamental constant (Li, Barrow & Mota 2010a) theories as well].

The organization of this paper is as follows. In Section 2 we give a brief summary of the major ingredients of the coupled scalar field model. In Section 3 we explicitly write down the models we are simulating and present a detailed description of our void-finding algorithm. Section 4 contains all our numerical results and finally Section 5 is devoted to a summary and conclusions.

2 THE BASIC EQUATIONS

All the equations relevant to the simulations here are derived and discussed in Li & Zhao (2009, 2010) and Li & Barrow (2010) but, for the present work to be self-contained, we shall still list the minimum set of them which is necessary for us to understand the underlying physics.

Instead of writing down the field equations directly as in some previous work, we start from a Lagrangian density

$$L = \frac{1}{2}\left[\frac{R}{\kappa} - \nabla^a\varphi\nabla_a\varphi\right] + V(\varphi) - C(\varphi)L_{\rm DM} + L_{\rm S} \tag{1}$$

in which R is the Ricci scalar, $\kappa = 8\pi G$ with G being the gravitational constant, $L_{\rm DM}$ and $L_{\rm S}$ are respectively the Lagrangian densities for dark matter and standard model fields and φ is the scalar field and $V(\varphi)$ its potential; the coupling function $C(\varphi)$ characterizes the coupling between φ and dark matter. Given the functional forms for $V(\varphi)$ and $C(\varphi)$, a coupled scalar field model is then fully specified.

Varying the total action with respect to the metric g_{ab}, we obtain the following expression for the total energy momentum tensor in this model:

$$T_{ab} = \nabla_a\varphi\nabla_b\varphi - g_{ab}\left[\frac{1}{2}\nabla^c\nabla_c\varphi - V(\varphi)\right] + C(\varphi)T^{\rm DM}_{ab} + T^{\rm S}_{ab}, \tag{2}$$

where $T^{\rm DM}_{ab}$ and $T^{\rm S}_{ab}$ are the energy momentum tensors for (uncoupled) dark matter and standard model fields. The existence of the scalar field and its coupling change the form of the energy momentum tensor, and thus could modify the cosmology from background expansion to structure formation.

Meanwhile, the coupling to scalar field produces a direct interaction (also known as the fifth force) between dark matter particles, due to the exchange of scalar quanta. This is best illustrated by the geodesic equation for dark matter particles

$$\frac{{\rm d}^2\boldsymbol{r}}{{\rm d}t^2} = -\nabla\Phi - \frac{C_\varphi(\varphi)}{C(\varphi)}\nabla\varphi, \tag{3}$$

where $\boldsymbol{r}$ is the position vector, t is the (physical) time, Φ is the Newtonian potential and ∇ is the spatial derivative. $C_\varphi = {\rm d}C/{\rm d}\varphi$. The second term in the right-hand side is the fifth force and only exists for coupled matter species (dark matter in our model). The fifth force also changes the clustering properties of the dark matter. Note that on very large scales φ could be considered as homogeneous and the fifth force vanishes.

It has become obvious that in order to implement the above two equations numerically, we need to solve both the time evolution and the spatial distribution of φ, and this could be done using the scalar field equation of motion

$$\nabla^a\nabla_a\varphi + \frac{{\rm d}V(\varphi)}{{\rm d}\varphi} + \rho_{\rm DM}\frac{{\rm d}C(\varphi)}{{\rm d}\varphi} = 0 \tag{4}$$

or equivalently

$$\nabla^a\nabla_a\varphi + \frac{{\rm d}V_{\rm eff}(\varphi)}{{\rm d}\varphi} = 0, \tag{5}$$

where we have defined

$$V_{\rm eff}(\varphi) = V(\varphi) + \rho_{\rm DM}C(\varphi). \tag{6}$$

The background evolution of φ can be solved easily once we know the current $\rho_{\rm DM}$, because $\rho_{\rm DM} \propto a^{-3}$. We can then divide φ into two parts, $\varphi = \bar{\varphi} + \delta\varphi$, where $\bar{\varphi}$ is the background value and $\delta\varphi$ is its (not necessarily small nor linear) perturbation, and subtract the background part of the scalar field equation of motion from the full equation to obtain the equation of motion for $\delta\varphi$. In the quasi-static limit in which we can neglect time derivatives of $\delta\varphi$ as compared with its spatial derivatives (which turns out to be a good approximation for our simulations, where the simulation box is much smaller than the observable Universe), we get

$$\nabla^2\varphi = \frac{{\rm d}C(\varphi)}{{\rm d}\varphi}\rho_{\rm DM} - \frac{{\rm d}C(\bar{\varphi})}{{\rm d}\bar{\varphi}}\bar{\rho}_{\rm DM} + \frac{{\rm d}V(\varphi)}{{\rm d}\varphi} - \frac{{\rm d}V(\bar{\varphi})}{{\rm d}\bar{\varphi}}, \tag{7}$$

where $\bar{\rho}_{\rm DM}$ is the background dark matter density.

With the $\rho_{\rm DM}$ made ready on some grid, we could then solve $\delta\varphi$ on that grid using a non-linear Gauss–Seidel relaxation method (in our simulations we have modified MLAPM, a publicly available N-body code using a self-adaptive refined grid so that high resolutions could be achieved in high-density regions). Because $\bar{\varphi}$ is also known, we then get the full solution of $\varphi = \bar{\varphi} + \delta\varphi$. This then completes the computation of the source term for the Poisson equation

$$\nabla^2\Phi = \frac{\kappa}{2}\left[C(\varphi)\rho_{\rm DM} - C(\bar{\varphi})\bar{\rho}_{\rm DM} + \delta\rho_{\rm B} - 2\delta V(\varphi)\right], \tag{8}$$

where $\delta\rho_{\rm B} \equiv \rho_{\rm B} - \bar{\rho}_{\rm B}$ and $\delta V(\varphi) \equiv V(\varphi) - V(\bar{\varphi})$ are respectively the density perturbations of baryons and scalar field (note that we

have neglected perturbations in the kinetic energy of the scalar field because it is always very small for our model).

We could then solve equation (8) using a linear Gauss–Seidel relaxation method on the same grid to obtain Φ. With both Φ and φ at hand, equation (3) could be used to compute the forces on the dark matter particles, and once we have the forces, we could do all the standard N-body operations such as momentum-kick, position-drift, time-stepping and so on.

Equations (2)–(8) are all that we need to complete an N-body simulation for coupled scalar field cosmology, and from that we could identify where the effects of the scalar-coupling come in.

(i) The influence of the modified cosmic background expansion rate mainly comes through the particle movements and time-stepping, i.e. equation (3). This is because in the simulations we shall use the scalefactor a as the time variable and $\mathrm{d}/\mathrm{d}t = \dot{a}\mathrm{d}/\mathrm{d}a$.

(ii) The varying-mass effect could be seen directly from equation (8), which shows that the contribution of the dark matter density $\rho_{\rm DM}$ to the source of the Poisson equation is multiplied by a factor $C(\varphi)$ which differs from 1 in general. In our model the mass of dark matter particles is not really varying, but the net effect is just that.

(iii) The fifth force appears explicitly on the right-hand side of the geodesic equation (3), but only for coupled matter species (dark matter in our model).

(iv) The velocity-dependent 'frictional force' is a bit subtler. It hides behind the fact that equations (3) and (7) are actually written in *different* gauges: equation (3) is the force for a dark matter particle and is given in that particle's rest frame, while equation (7) is written in the fundamental observer's frame. As a result, to use the $\delta\varphi$ solved from equation (7) in equation (3), we need to perform a frame transform $\nabla\delta\varphi \rightarrow \nabla\delta\varphi + a\dot{\bar{\varphi}}\dot{\boldsymbol{x}}$ in which $\dot{\boldsymbol{x}}$ is the comoving velocity of the said particle relative to the fundamental observer. This force is thus expressed as $-\frac{C_\varphi}{C}a\dot{\varphi}\dot{\boldsymbol{x}}$, and obviously the faster a particle travels the stronger the frictional force it feels.

In our numerical simulation, we have included all these effects consistently (Li & Barrow 2010). In particular, we have computed the fifth force explicitly, rather than simply assuming that it is always proportional to gravity: as shown in Li & Zhao (2009, 2010), such an assumption could be fairly poor for certain models where the scalar field configuration is very inhomogeneous, although it is good enough for other models (Li & Barrow 2010).

3 SIMULATIONS AND VOID-FINDING ALGORITHM

3.1 The models studied

In this work we consider the voids in the two different coupled scalar field models studied respectively by Li & Barrow (2010) and Li & Zhao (2009, 2010); Zhao et al. (2010). Both models have an exponential coupling between dark matter and the scalar field φ,

$$C(\varphi) = \exp(\gamma\sqrt{\kappa}\varphi) \tag{9}$$

and runaway potentials for φ:

$$V(\varphi) = \frac{\Lambda}{\left(\sqrt{\kappa}\varphi\right)^\alpha} \tag{10}$$

for the model of Li & Barrow (2010), and

$$V(\varphi) = \frac{\Lambda}{\left[1 - \exp\left(-\sqrt{\kappa}\varphi\right)\right]^\alpha} \tag{11}$$

for the model of Li & Zhao (2009, 2010). In the above, Λ is a parameter of mass dimension 4 and is of the order of the present density for dark energy (φ plays the role of dark energy in the models); its precise value is determined by the numerical code for the consistency in the background cosmology (Li & Barrow 2010). γ and α are dimensionless model parameters controlling respectively the strength of the coupling and the steepness of the potentials.

Table 1. A summary of the details of the models studied here. For all the runs: $\Omega_{\rm m} = 0.257$, $n = 0.963$, $\sigma_8 = 0.769$, $H_0 = 71.9$ km s^{-1} Mpc^{-1}; size of simulation box is $64h^{-1}$ Mpc and particle number is 256^3 so that mass resolution is $1.04 \times 10^9\, h^{-1}\, \mathrm{M}_\odot$; domain grid has 128 cells on each side, and the finest refinement has 16 384 cells on each side, leading to a force resolution of $\sim 12\, h^{-1}$ kpc. L, N, C stand for ΛCDM, non-chameleon and chameleon, respectively.

Model	$V(\varphi)$	$C(\varphi)$	γ	α	$\kappa\Lambda/3H_0^2$
L	constant	1	0.0	0.0	0.743
N1	equation (10)	equation (9)	−0.05	0.1	0.717
N2	equation (10)	equation (9)	−0.10	0.1	0.781
N3	equation (10)	equation (9)	−0.15	0.1	0.838
N4	equation (10)	equation (9)	−0.20	0.1	0.891
C1	equation (11)	equation (9)	0.5	1.0×10^{-6}	0.743
C2	equation (11)	equation (9)	0.5	1.0×10^{-5}	0.743
C3	equation (11)	equation (9)	1.0	1.0×10^{-6}	0.743
C4	equation (11)	equation (9)	1.0	1.0×10^{-5}	0.743

For the potential equation (10) we choose $\alpha = 0.1$ and $\gamma < 0$ so that the total effective potential $V_{\rm eff}(\varphi)$ is of runaway type. The scalar field then rolls quickly at early times [$\varphi_{\rm today} - \varphi_{\rm early} \sim \mathcal{O}(M_{\rm Pl})$ with $M_{\rm Pl}$ the Planck mass], until slowing down to the slow-roll regime, when it behaves like a normal quintessence field. For the potential in equation (11) we choose $\alpha \ll 1$ and $\gamma > 0$, which ensures that $V_{\rm eff}$ has a global minimum close to $\varphi = 0$ and $\mathrm{d}^2V_{\rm eff}(\varphi)/\mathrm{d}\varphi^2 \equiv m_\varphi^2$ at this minimum is very large in high-density regions; then φ is trapped close to 0 all through the cosmic history. These two cases are two extremes of the coupled scalar field: in the former φ clusters very weakly just as in normal quintessence, and the fifth force is, to a good approximation, always proportional to gravity; the scalar field coupling also drastically modifies the background cosmology and structure formation at early times [$z \sim \mathcal{O}(10^2)$]. In the latter case φ is very inhomogeneous and the fifth force is greatly suppressed in high-density regions where φ acquires heavy mass, $m_\varphi^2 \gg H^2$ (H is the Hubble expansion rate), and thus the fifth force cannot propagate far. The suppression of the fifth force is even severer at early times, meaning that the structure formation is only influenced at late times (z less than a few); also, because φ is trapped close to 0 all the time, the background cosmology is forced to be indistinguishable from ΛCDM. In Table 1 we summarize the details for all the models we study here.[1]

3.2 Void-finding algorithm

Following Colberg et al. (2005), our void-finding algorithm consists of two steps: the identification of spherical protovoids and the

[1] For clearness we shall refer to the model with equation (11) as chameleon model, because here the scalar field mass m_φ depends sensitively on its environment and fluctuates strongly from point to point, and correspondingly the model with equation (10) as the non-chameleon model because here m_φ is largely ignorant of the environment. The formal definition of a chameleon model (Khoury & Weltman 2004; Mota & Shaw 2007) is not relevant to our discussion in this work.

mergers of protovoids to form voids of arbitrary shape (all through this paper protovoids and voids are different things and are not to be confused).

The protovoids are spherical regions in which the average of the density contrast $\delta = \rho/\bar{\rho} - 1$ is below some pre-defined threshold $\delta_{\rm v}$. As shown by Colberg et al. (2005), voids very clearly correspond to the troughs of the initial density field, justifying the assumption that voids grow gravitationally from the initial negative overdensities. Assuming a spherical evolution model for the voids (Gunn & Gott 1972; Dubinski et al. 1993), the growth of the voids can be studied analytically, and it is found that at the time of shell-crossing the overdensity inside the spherical protovoid reaches -0.8. Although this is the result for Einstein–de Sitter cosmology (Colberg et al. 2005), we shall adopt it as a guidance and set $\delta_{\rm v} = -0.8$ in the coupled scalar field models as well.

Our void-finding algorithm is similar to that of Colberg et al. (2005), but it differs from the latter in various details, particularly the treatment of the mergers of protovoids. To be clear and self-contained, here we briefly describe our algorithm in separate steps.

(1) A regular $128 \times 128 \times 128$ mesh is set up and the particle densities on this mesh are computed using the Triangular-shaped Cloud (TSC) scheme. This scheme ensures that the density interpolation is smoother than the usually used Cloud-in-Cloud scheme.

(2) The local minima in the density field are located, and these are considered as the centres of the protovoids (van de Weygaert & van Kampen 1993). Top-hat spherical windows with large enough radii so that the smoothed density contrasts inside are greater than $\delta_{\rm v}$ are then placed at these minima, and the radii are gradually decreased until the density contrast drops below $\delta_{\rm v}$. These minima and radii are then taken as the centres and sizes of the protovoids, respectively. One can also do this for all grid points on our mesh (i.e. set up a top-hat window on each grid point, decrease the radii of the windows until the overdensity at a grid point falls below $\delta_{\rm v}$) as in Keselman et al. (2010), but this is more time-consuming and we have checked that the two methods lead to compatible results.

(3) The above-identified protovoids are merged as appropriate to form the final voids of arbitrary shapes. It is well known that voids occupy the majority of the space, with islands of matter (dark matter haloes and galaxies) interconnected by the narrow filaments that go through them. As a result, the merging criteria must be chosen carefully: for example, the dumb-bell-shaped configurations are better to be avoided (Colberg et al. 2005) to prevent the protovoids from all being merged to form a single void as big as the simulation box. To this end let us adopt a variant of the merging criterion proposed by Colberg et al. (2005), which consists of the following steps.

(i) Consider all the protovoids which have not been assembled into any final voids. Find the biggest one, which is the primary progenitor of a merged void-to-be, and all the smaller ones that intersect it.

(ii) If a smaller protovoid fully lies within the biggest one, then it is removed from the list.

(iii) *All* the smaller protovoids whose centres lie inside the biggest one are merged to the latter.

(iv) *All* the smaller protovoids whose centres lie outside the biggest one while still having significant intersection with the latter are merged into the latter. There are certain freedoms as for what is to be considered as significant, and here we will adopt the proposal of Colberg et al. (2005): we divide the line segment connecting the centres of the smaller and the biggest protovoids into three sections, a section a which lies in both spheres and two sections b, c lying only in one of the two spheres, respectively. The intersection is only considered to be significant if $|a| \geqq \max(|b|, |c|)$.

(v) *All* the smaller protovoids which do not satisfy $|a| \geqq \max(|b|, |c|)$ are *not* merged into the biggest one. In this case, the portion of volume shared by the smaller and the biggest protovoids is assigned to the latter, and the volume of the smaller protovoid is decreased correspondingly. The smaller protovoids are however not removed from the list but will be the building blocks for the voids-to-be considered later (as are the protovoids which have no intersections with the currently biggest one).

(vi) The total volume of the final merged void is that of the union of the biggest protovoid and *all* those smaller ones merged to (eaten by) it.[2] By our construction the shape of the final void could be arbitrary, but as Colberg et al. (2005) we define an effective radius $r_{\rm eff}$ such that $\frac{4\pi}{3} r_{\rm eff}^2$ equals the volume of it. The centre of the merged void, on the other hand, is taken to be the volume average of the centres of all merging blocks.

(vii) The biggest protovoid and all the smaller ones eaten by it [but *not* the ones dealt with in step (v) above] are considered to be already assembled, and are excluded from the future runs of the merging process. Steps (i)–(vii) are then repeated until all the protovoids are assembled.

Note that using this algorithm we could naturally avoid the dumb-bell-shaped configurations for which two big protovoids are connected by thin tunnels and are finally merged, because the two big protovoids have no intersection by definition, and are thus treated separately. The multiple merges, in contrast with the algorithm of Colberg et al. (2005) which stops looking for further overlaps once it has found one, could produce bigger voids, for which the biggest protovoids typically eat tens of smaller ones, thereby expanding significantly.

In this work we only consider voids whose effective radius $r_{\rm eff} \geq 2.0\,h^{-1}$ Mpc, which is four times the size of the cells in the void-finder grid (Colberg et al. 2005). As the majority of the voids are small ones, this will inevitably leave voids smaller than the above threshold undetected, as a price of maintaining accuracy.

Another issue concerning the search for voids is the *void-in-clouds* situation discussed by Sheth & van de Weygaert (2004), i.e. smaller voids embedded in overdense regions may not merge with or be absorbed by other voids in the hierarchical evolution, but can collapse as the overdense region is squeezed. In our algorithm, the voids in clouds are not treated separately. Indeed, the algorithm simply searches for the local density minimum regardless of its environment, and tries to find neighbouring protovoids which it can potentially merge with (if there are no neighbouring protovoids, then just leaves it alone). Therefore, in principle our method can also locate those voids in haloes. However, because such voids are mostly rather small (as they are smaller

[2] The volume is computed as follows: we distribute a big number of points evenly in the whole volume so that the number density n is known, and then count the number N of points which lie inside the union. The volume of the union is then simply N/n. With our choices of the number density, we find that the numerical results agree with analytical predictions (where the latter are available) typically better than 99.9999 per cent. We are also careful to avoid assigning the same portion of space to more than one merged void: for example, when computing the volume of a void-to-be, we always exclude the parts that lie in any of the previously identified voids.

than their hosting haloes) many of them will be missed in this work.

3.3 Other void-finding algorithms

Unlike that for haloes, the definition for voids is not unequivocal and the lack of a consensus has led to many different definitions. Accordingly, there have been various void-finding algorithms, differing in the working mechanisms, performances and complexities.

The algorithm used in this work, and its original form (Colberg et al. 2005), are based on dark matter distribution, as they search voids in the dark matter density field; the voids found with these methods are irregularly shaped underdense regions around local density minima. In the same class are the algorithms of Plionis & Basilakos (2002) and Shandarin et al. (2006), where the voids are found by searching underdense cells from a grid and appropriately connecting them, and those of Platen, van de Weygaert & Jones (2007) and Neyrinck (2008), which use spatial tessellation techniques (Schaap & van de Weygaert 2000) as the infrastructure to construct the density field, and the watershed concept to define voids.

Another class of void-finding algorithms are based on the distributions of dark matter haloes or even galaxies, because they search voids from a set of points (haloes or galaxies) (Hoyle & Vogeley 2002; Brunino et al. 2007; Foster & Nelson 2009). The algorithms based on galaxy distribution are very convenient to locate voids in an observed galaxy catalogue; when applied to simulated galaxy catalogues, one has to bear in mind that baryonic physics is still not very well understood.

Colberg et al. (2008) recently made a comparison of various void-finding algorithms by applying them to the same simulation output. Although they agree qualitatively, their quantitative predictions are shown to be quite different. This is certainly not surprising, not only because the working mechanisms and underlying parameters (such as the criterion of void overdensity) are different, but also because different methods search for voids from different underlying fields: it is known that galaxies are biased tracers of dark matter haloes, which are themselves biased tracers of the dark matter density field. There does not appear to be a best algorithm, but only the most appropriate or convenient one, depending on the underlying field etc. This said, certain algorithms (Platen et al. 2007; Neyrinck 2008) do appear to fit better with visual impression (Colberg et al. 2008), which is perhaps not unexpected, given that the tessellation techniques used there produce the 'most local possible estimate of the density field which bears meaningful information' (Neyrinck 2008).

Given that different methods could produce quite different quantitative results, we shall only compare our results with Colberg et al. (2005), which our algorithm is based on. Such a comparison is deferred to Section 4.3, where we can see that there is a reasonable agreement.

As in Colberg et al. (2005), we cannot straightforwardly compare the results with those obtained from analyses for voids traced in dark matter halo or galaxy distributions, or from analyses of observational data, which we hope to address in future higher-resolution simulations with bigger simulation boxes and hydrodynamics included. On the other hand, Colberg et al. (2005) found that their void-finding algorithm based on the dark matter distribution did produce a void size distribution which agreed reasonably with what had been found from galaxy catalogue, which is reassuring, given our agreement with Colberg et al. (2005). We will briefly comment on the possible implications for our C and N models below.

4 NUMERICAL RESULTS

Having introduced the models and the void-finding algorithm in the above section, we now present and discuss the numerical results.

4.1 Preliminary results

Some preliminary results to provide a visual impression are given in Fig. 1; here we select a thin slice from our simulation box and output the particle distribution at various different redshifts. For simplicity we shall only do this for the models L, N4 and C4, and redshifts $z = 3, 2, 1, 0$. The central region of the slice harbours a large underdensity as can be easily spotted by eye, and as time passes (from left-hand to right-hand panels) this underdensity grows significantly. The difference between the growth rates for different models is clearly visible: at $z = 3$ the particle distributions are visually indistinguishable for all models; at $z = 2$ they are almost identical for models L and C4 because the fifth force in C4 is still severely suppressed and has negligible effects, while in N4 model the underdensity is slightly bigger because the fifth force, unsuppressed, boosts the clustering of matter; by $z = 1$ the difference in the particle distributions for all models has become clear, with the biggest underdensity being in model N4, followed by models C4 and L; this trend only becomes stronger at $z = 0$.

This suggests that voids do grow at different rates in different coupled scalar field models. To see this point more clearly, we have added to Fig. 1 the voids identified using the above-mentioned algorithm. For clarity we only show the voids that have intersection with the middle of the selected slice, and only do it for $z = 1, 0$. As explained above, our voids generally have irregular shapes, but we only treat them as spherical, assuming the radius to be $r_{\rm eff}$; the circles in Fig. 1 are the intersections between the voids and the middle plane of the selected slice.

The voids in Fig. 1 generally fit the underdense regions spotted by eye, showing that the void-finding method works reasonably well. Some seemingly strange features, e.g. some voids intersecting or containing others, are artificial because we treat irregular voids as spherical and only plot the intersections between voids and the selected slice (Colberg et al. 2005). There seem to be some underdense regions which are not populated by voids, but this is because we only plot a very thin slice ($0.1\,h^{-1}$ Mpc) of the simulation box or, again, we treat voids as spherical (Colberg et al. 2005).

As expected, we find that the voids end up bigger in the N4 models than in the C4 and L models. In particular, at $z = 0$ the biggest N4 void is significantly bigger than its counterpart in model L, as it has eaten many more small protovoids.

4.2 Probability distribution of density contrast

As is shown in Li & Barrow (2010), Li & Barrow (in preparation) and Li & Zhao (2009, 2010), the existence of the scalar field and its coupling to dark matter efficiently enhance the clustering of matter, and we thus expect that an associated effect is the fast evacuation of the low-density regions, resulting in a bigger portion of the space being inside voids (than in ΛCDM model).

To give a first check of this expectation, we consider the probability distribution of the density contrast, which shows how much of the total space is in overdense/underdense regions. To obtain this, we place top-hat windows with radius $2.0\,h^{-1}$ Mpc at each of our 128^3 regular grid points and compute the smoothed density inside them. We then count the number of grid points at which the density

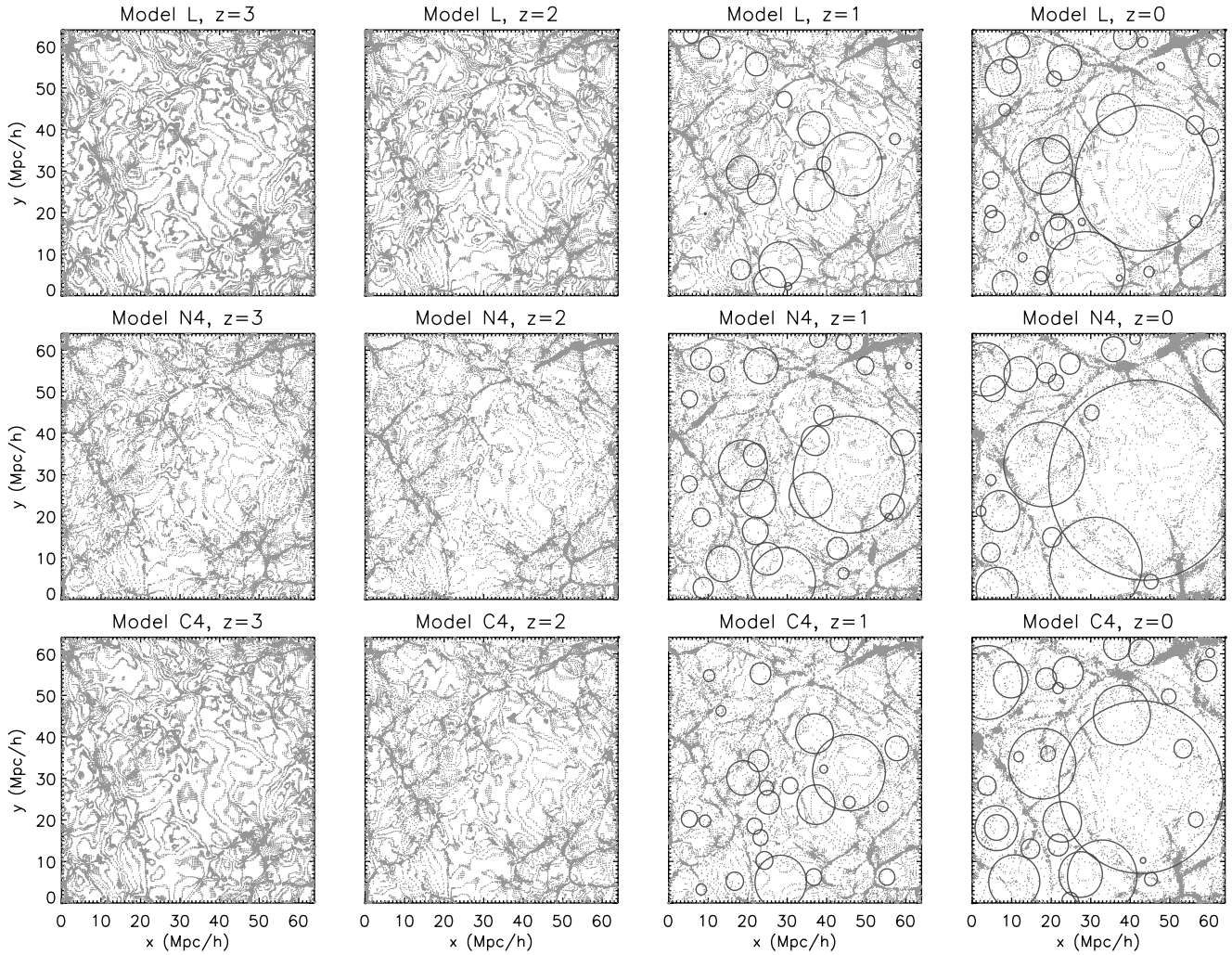

Figure 1. Visual impression. Shown are the particle distribution in a thin slice (with thickness $0.1\,h^{-1}$ Mpc) taken from the simulation boxes for the models L (upper row), N4 (middle row) and C4 (lower row), at four different output redshifts $z = 3$, 2, 1 and 0 (from left to right columns). Periodic boundary condition in the particle distribution has been used to shift the origin so that the biggest void is roughly at the centre. For redshifts 1 and 0 the voids which intersect the thin slice are superposed (see text for details) for comparison. The horizontal and vertical axes respectively represent the x and y coordinates.

contrast δ falls within $[\delta_0, \delta_0 + d\delta]$, and divide this by 128^3 to obtain the probability that $\delta \in [\delta_0, \delta_0 + d\delta]$.

The results for our nine models are summarized in Fig. 2 (see the figure caption for a detailed description), from which we could see clearly the trend that the coupling scalar field models (both N and C) predict more higher and lower density regions than ΛCDM (L). However, there are some notable differences between them, reflecting the fact that the N and C models are qualitatively different.

For the C models, as mentioned above, the scalar field φ is trapped at the minimum of $V_{\rm eff}$, φ_*, which is close to 0 all through the cosmic history (as can be easily checked using the equation below). Using this fact it could be straightforward to find that

$$\sqrt{\kappa}\varphi_* \approx \frac{\alpha\Lambda}{\gamma\rho_{\rm DM}},$$

and thus (Li & Zhao 2009)

$$m_\varphi^2 = \frac{\partial^2 V_{\rm eff}}{\partial\varphi^2}(\varphi_*) \approx \frac{(\gamma\kappa\rho_{\rm DM})^2}{\alpha\kappa\Lambda}. \quad (12)$$

Although in reality the fifth force is quite complicated because the force between two particles depends on the matter distribution between them, the quantity m_φ nevertheless could be utilized to qualitatively understand the underlying physics. Basically, the greater the m_φ, the shorter the distance the fifth force could propagate, which means that a particle will feel the fifth forces exerted by less particles: in short, a heavy mass m_φ could *suppress* the fifth force.

From equation (12), we see that m_φ increases as γ, $\rho_{\rm DM}$ increase or α decreases, and vice versa. Thus we expect the fifth force to be more severely suppressed in models C1, C3 in which α is smaller than in models C3, C4; within C1, C3 it is more suppressed for C3 for which γ is bigger, and for all models it is more suppressed at a higher redshift, where $\rho_{\rm DM}$ is bigger overall (Li & Zhao 2009, 2010). Furthermore, $\rho_{\rm DM}$ is generally lower in the void regions, where the fifth force is expected to be less suppressed.

In Fig. 2 we could see that at $a = 0.5$ (redshift 1, lower right panel) the probability distributions of the larger density contrasts for the models C1–C4 are essentially the same as in model L, because fifth force is strongly suppressed there and then. On the other hand, for lower-density contrasts in the low-density regions, we do see the deviations from model L increasing for a decreasing m_φ, as expected. As time passes, m_φ decreases overall and by $a = 1.0$ (redshift 0, upper right panel) a significantly greater portion

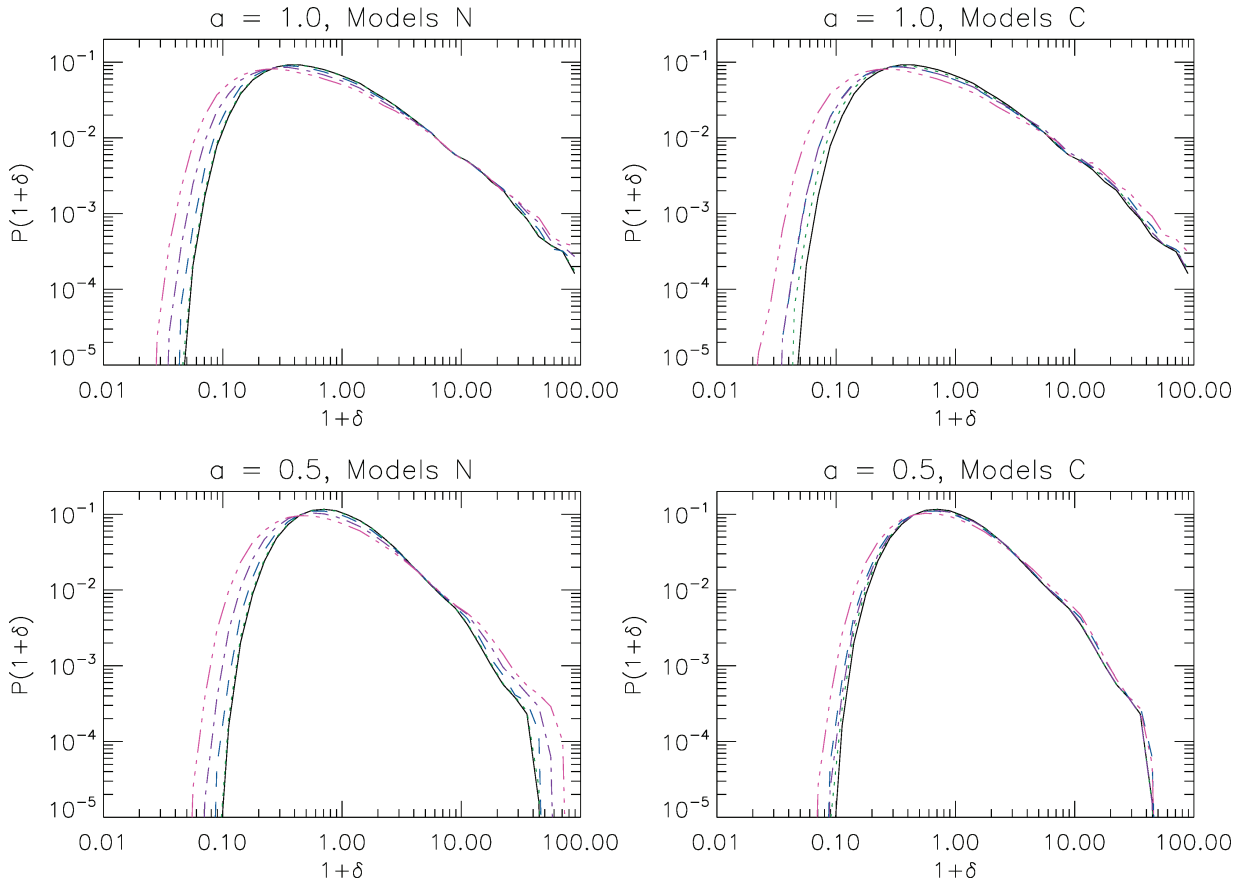

Figure 2. The probability distribution of the density contrast δ (equivalently $1 + \delta$). Upper left panel: Results at redshift 0 for the non-chameleon models N1 (green dotted curve), N2 (blue dashed curve), N3 (purple dot–dashed curve) and N4 (pink dot-dot-dot-dashed curve) in contrast to the ΛCDM (L) result (black solid curve). Upper right panel: The same but the green dotted, blue dashed, purple dot–dashed and pink dot-dot-dot-dashed curves now represent respectively the models C1, C2, C3 and C4. Lower left panel: The same as the upper left panel but for redshift 1. Lower right panel: The same as the upper right panel, but for redshift 1.

of space will be evacuated in the C models than in the L model, and meanwhile the enhancement in the clustering of matter due to the (attractive) fifth force increases the chance that the peaks in the initial density field develop into highly overdense regions ($\delta \gg 1$, the increases are however not very significant, mainly because the fifth force is suppressed in the high-density regions and its power is largely unrealized).

For the N models, equation (12) does not apply because the scalar field always rolls down the effective potential $V_{\rm eff}$. m_φ^2 does not fluctuate strongly in space, and the fifth force is never severely suppressed (Li & Barrow 2010). As a result, the fifth force starts to affect the structure formation at a fairly early time. As is shown in Fig. 2, by $a = 0.5$ (redshift 1, lower left panel) there have been significantly more overdense *and* underdense regions than L model, mainly because the fifth force helps the transfer of more matter from low-density to high-density regions.[3]

At $a = 1.0$, however, although the N models still predict larger evacuated space than L model does (upper left panel), the volumes of space in the very overdense regions ($\delta \gg 1$) are less different between the N and L models, the reason of which is, as more and more matter is transferred to the high-density regions, less and less matter remains in the empty regions to be pumped: even though the aggregation of matter into high-density regions starts earlier in the N models, it slows down eventually as matter in the low-density regions is used up, and there turns out to be time for the L model to catch up somehow. But note that the effect of the fifth force is actually not that important: for example, the fifth force is about 0.08 times the gravitational strength, while the varying-mass effect is stronger because $C(\varphi)$ can be as small as 0.7 at late times Li & Barrow (in preparation); besides, the modified expansion rate also changes the clustering of matter. All these effects could play a role here.

The results for our N models are qualitatively similar to that of the ReBEL model (Nusser, Gubser & Peebles 2005) as investigated by Keselman et al. (2010) and Hellwing & Juszkiewicz (2009).

4.3 Volume of voids

Having seen above that the fifth force in both the N and C models helps evacuate the low-density regions, we now look at how the void properties are affected.

The first interesting quantity is the void volume function (similar to the halo mass function in the studies of the statistical properties of dark matter haloes), which shows the number density of voids to be larger than a given volume V. Fig. 3 displays our results for the N, C and L models. For comparison we also superimpose some

[3] Note that the probability is higher in the N models than in the L model for both $1 + \delta \gg 1$ and $1 + \delta \ll 1$, as the total amount of matter is the same in both models.

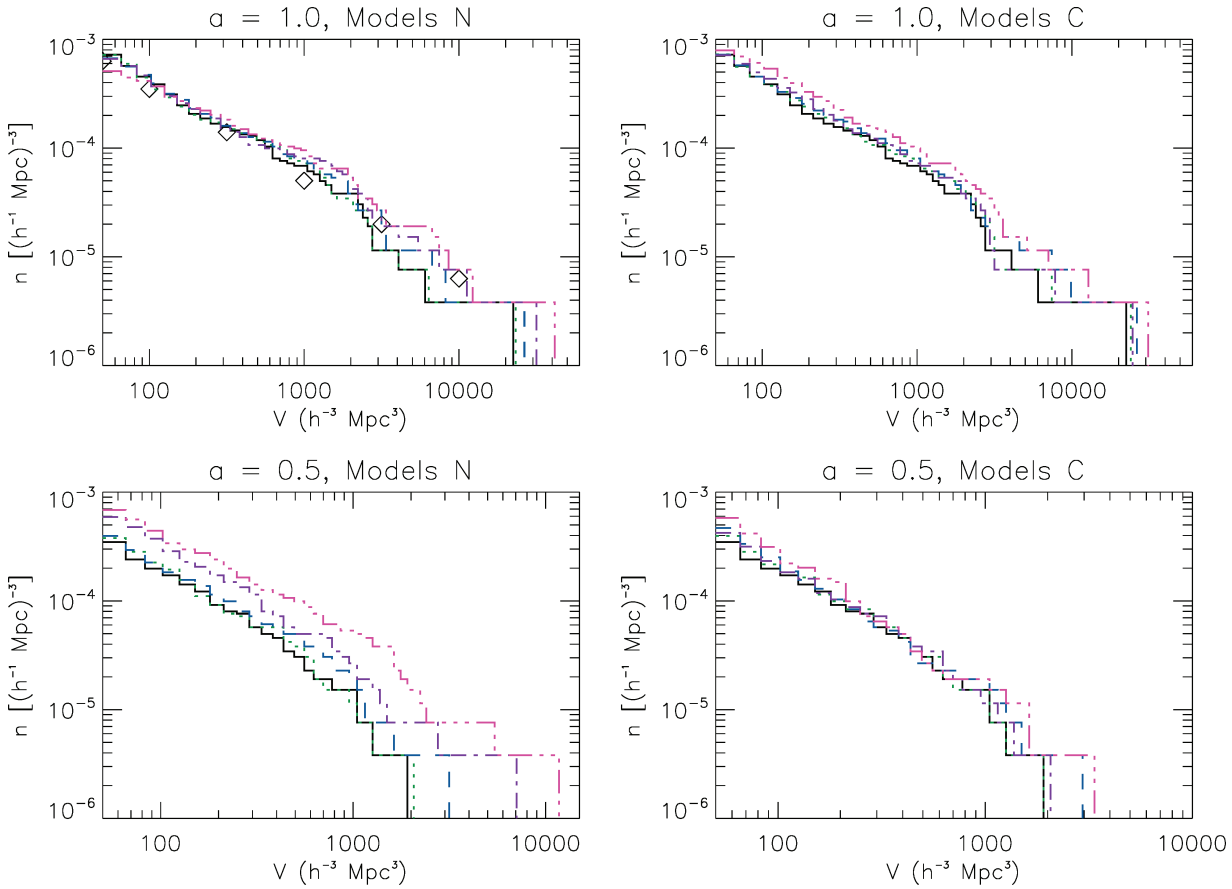

Figure 3. The void volume functions for the simulated models. Upper left panel: Results at redshift 0 for the non-chameleon models N1 (green dotted curve), N2 (blue dashed curve), N3 (purple dot-dashed curve) and N4 (pink dot-dot-dot-dashed curve) in comparison to model L (black solid curve). Upper right panel: The same, but the green dotted, blue dashed, purple dot–dashed and pink dot-dot-dot-dashed curves now stand for model C1, C2, C3 and C4, respectively. Lower left panel: The same as the upper left panel but for redshift 1. Lower right panel: The same as the upper right panel, but for redshift 1. In all the plots the horizontal axis is the void volume V, in unit of $(h^{-1}\,\mathrm{Mpc})^3$, and the vertical axis is the number density of voids which are larger than V, in unit of $(h^{-1}\,\mathrm{Mpc})^{-3}$. For comparison we have also superimposed, in the upper left panel only, the void volume function for ΛCDM model taken from Colberg et al. (2005), as shown by the diamonds.

ΛCDM data points taken from Colberg et al. (2005) in the upper left panel, which show reasonable agreement with our result for the L model (given the minor differences in the algorithm, the different particle dumps used and more importantly the different simulation box sizes [our simulation box is only about 1/8 as theirs (they used GIF simulations) and so the results are not very reliable for the largest voids].

Understandably, the more strongly the matter particles cluster, the more effectively the low-density regions are evacuated and therefore the bigger the sizes of the voids tend to be. In the N models, not only does the fifth force, which is unsuppressed, start to take effect earlier, but also the universe expands more slowly, leaving more time for particles to clump (Li & Barrow 2010) and Li & Barrow (in preparation). Consequently, by $a = 0.5$ (Fig. 3, lower left panel), we see large increases in both the void number density and the void size in the N models as compared to the L model (for example, the number density could be twice as high).

As time goes on, low-density regions are largely emptied and enlarged due to the faster expansion rate than the background (and overdensities). If the void is a simple spherical underdensity embedded in an otherwise homogeneous and large-enough universe, then its expansion rate is slower after the shell-crossing (Blumenthal et al. 1992) but the expansion will still go on. In the simulations, the voids expand while squeezing matter in between them, and there will be a point when they cannot further squeeze matter easily, by which they will have occupied the majority of the space (cf. Fig. 1, the right-most panels). The voids then stop growing (in the comoving coordinates; for example, the biggest void in Fig. 1 cannot grow to a size which is bigger than the simulation box). As a result, when voids in the N models stop growing, those in the L model are still in the process. Finally, at $a = 1.0$, the void volume function of the L model more or less catches up those in the N models, as is evident in the upper left panel of Fig. 3. We also note that at $a = 1.0$ there are less small voids in the N4 model than in the L and other N models, which is likely because of the fact that small voids have been used up to merge to form bigger ones.

For the C models, the suppression of the fifth force means that the clustering of matter and growth of voids are less affected by it. One might think that, from equation (12), m_φ could be quite light in low-density regions and thus the fifth force should be essentially unsuppressed there. The point, however, is that equation (12) is only used to understand the physics intuitively, and in reality the fifth force is proportional to $\nabla\delta\varphi$ (cf. equation 3) with $\delta\varphi$ determined by the dynamical equation (7). As a result, the value of $\delta\varphi$ in void regions generally depends on that outside the regions in the way that the solution to a differential equation depends on its boundary

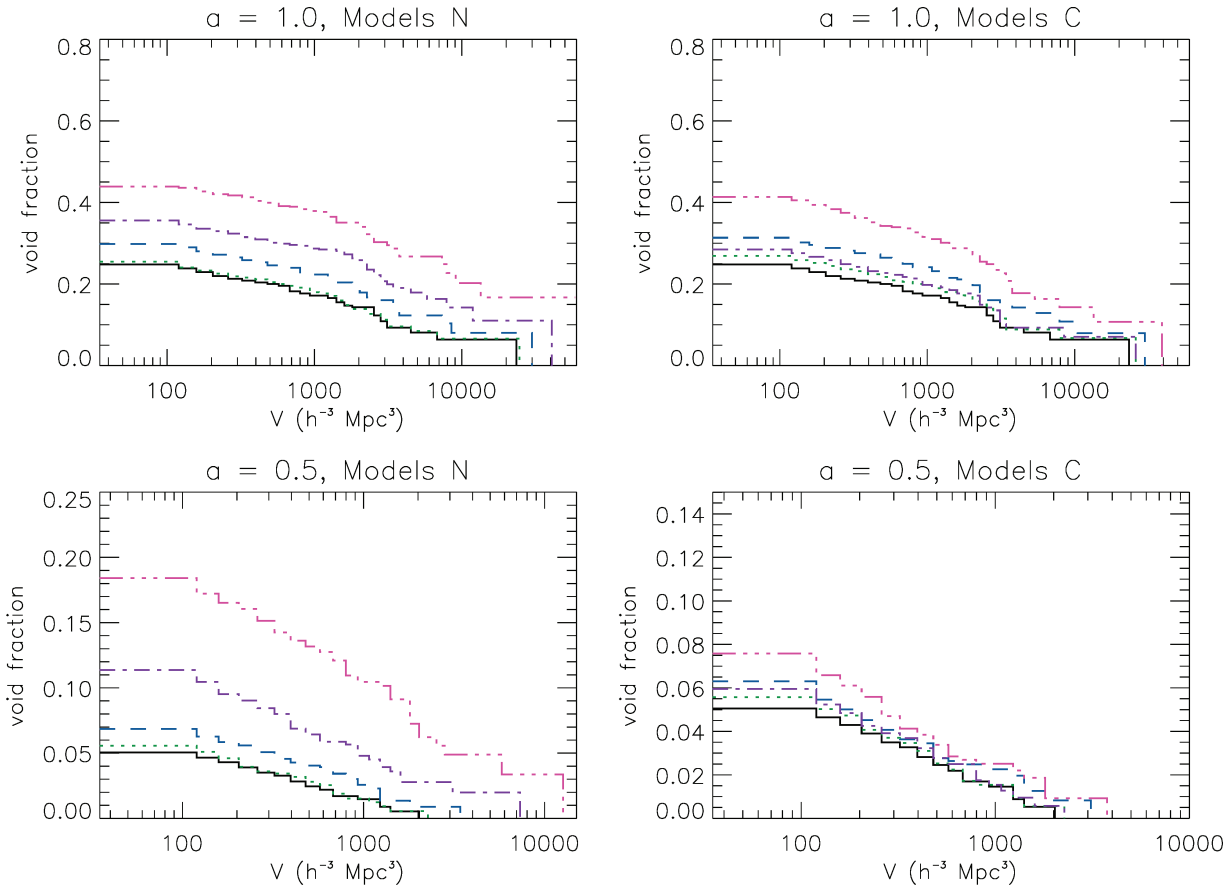

Figure 4. The fraction of the total space that is occupied by voids larger than V as a function of V. Upper left panel: Results at redshift 0 for the non-chameleon models N1 (green dotted curve), N2 (blue dashed curve), N3 (purple dot–dashed curve) and N4 (pink dot-dot-dot-dashed curve) in comparison to model L (black solid curve). Upper right panel: The same, but the green dotted, blue dashed, purple dot–dashed and pink dot-dot-dot-dashed curves now stand for model C1, C2, C3 and C4, respectively. Lower left panel: The same as the upper left panel but for redshift 1. Lower right panel: The same as the upper right panel, but for redshift 1. In all the plots the horizontal axis is the void volume V, in unit of $(h^{-1}\,\mathrm{Mpc})^3$, and the vertical axis is the fraction of space occupied by voids larger than V.

conditions. This is easily seen in the $a = 0.5$ case (Fig. 3, lower right panel), which shows that the void volume functions for the C models do not deviate much from those for the L model (one might appreciate the effect of the suppression of the fifth force by considering that the ratio between the magnitudes of fifth force and gravity is $2\gamma^2$ if the former is not suppressed, and $\gamma \sim \mathcal{O}(0.1)$ for N models while $\gamma \sim \mathcal{O}(1)$ for C models).

We could also have an examination of the void filling factor, defined as the fraction of total space that is filled by voids which are either bigger or smaller than V. Because our algorithm leaves the very small voids undetected, we choose to show the former, and the results are given in Fig. 4. It turns out that this plot shows more clearly the effects of the scalar coupling. As our first example, for the L model at $a = 0.5$ (Fig. 4, lower left panel), we notice that only 5 per cent of the total space is filled by voids larger than $35\,h^{-3}$ Mpc^3, in contrast to more than 11 and 18 per cent for the models N3 and N4, respectively. At $a = 1.0$, as a result of void growth and mergers, the numbers for these three models change to 25, 35 and 45 per cent, respectively.

For the C models (Fig. 4, right-hand panels), we obtain qualitatively similar results, but the deviations from model L are obviously smaller due to the suppressing of the fifth force. For example, at $a = 0.5$, the fraction of space occupied by voids larger than $35h^{-3}$ Mpc^3 is respectively 5, 6 and 7.5 per cent for the models L, C3 and C4, while at $a = 1.0$ these numbers become 25, 28 and 41 per cent.

In both classes of models, the scalar field coupling dramatically changes the total volume of void regions, and could potentially affect the properties of matter and galaxy distribution in voids. It is known, for example, that the void halo mass function has both different shape and different normalization from the total mass function (Colberg et al. 2005), in agreement with the analytic studies about the dependence on local density (Mo & White 1996; Sheth & Tormen 2002) for the L model. Not surprisingly, the mass functions is lower in the void regions. For the coupled scalar field models, due to the faster and more complete evacuation of underdense regions, it is possible that we get even lower mass functions for haloes in voids. We plan to investigate this in more details using simulations with higher spatial and mass resolutions in the future.

For the properties of void galaxies, Patiri et al. (2006) performed a study using the galaxies in voids identified from observational data and compared with those from the Millennium run semi-analytic galaxy catalogue. They found that the void galaxies appeared to be bluer on average, which agreed with previous studies (Benson et al. 2003), but also that the environment (i.e. whether they are inside voids or not) had very limited impacts on the properties of galaxies such as the colour distribution, concentrations and star formation rate. One thing to notice is that void galaxies are arranged

in small groups rather than randomly, and thus the local density is not necessarily significantly lower than the environments for galaxies outside voids. It could be interesting to see if these all remain true for coupled scalar field models, for which the distribution of matter and thus of galaxies in voids is expected to be modified as mentioned above. For these one needs either more elaborate simulations or a generalization of the semi-analytical formulae developed for model L (Mo & White 1996; Sheth & Tormen 2002; Benson et al. 2003; Sheth & van de Weygaert 2004) to models C and N.

If we had chosen void-finding algorithms based on halo or even galaxy distributions, the above qualitative features are expected to remain. Although not perfect because of the biases, haloes and galaxies are reasonable tracers for the dark matter distribution. For example, it is known that galaxies are mainly concentrated in the thin walls surrounding the voids, while they are rarer inside, which agrees with the dark matter distribution [see fig. 1 of Colberg et al. (2008) for a visual example]. For the coupled scalar field models, the excessive expansion of voids means galaxies will be squeezed more than in model L, and the faster growth of voids should be reflected in the galaxy distributions.

Finally, as mentioned in Section 3.2, there are also voids in the haloes, many of which are missed in our simulations because we have only considered voids whose effective radii are larger than $2h^{-1}$ Mpc. These voids generally collapse as the matter clusters (Sheth & van de Weygaert 2004), rather than merging with other voids during the hierarchical evolution. In the coupled scalar field models, because matter clusters faster and more strongly, we expect that these voids get squeezed more quickly and disappear sooner. This is not a concern here but certainly should be taken care of in studies with higher resolutions when comparing the observed void volume distribution with predictions.

4.4 Void density profiles

The next quantity we are interested in is the void density profile, which characterizes how matter is distributed within the empty regions. Like the growth rate of voids, this is also interesting and bears information about the physics driving the structure formation. In Keselman et al. (2010), for example, it is shown that the ReBEL model could produce different density profiles inside the void: the profile is steeper than the ΛCDM prediction, and is more so for smaller voids. In this subsection we would like to see what happens for our coupled scalar field models.

As our voids are made from the spherical protovoids and thus in principle could have an arbitrary shape, it is difficult to give well-defined profiles for them. Instead, because we are only interested the steepness at the boundaries of the empty regions, here we choose to compute the profiles for the *protovoids*, which are simply obtained by varying the radii of the top-hat smoothing windows located at the centres of the protovoids and calculating the average densities inside them.

As Keselman et al. (2010) have done, we will consider two groups of the (proto-)voids, with radius ranges of $6 \leq r_0/(h^{-1}\,\mathrm{Mpc}) \leq 9$ and $4 \leq r_0/(h^{-1}\,\mathrm{Mpc}) \leq 6$, respectively, where r_0 is the radius of the protovoid.

For the group of larger voids, with radii in the range $6 \leq r_0/(h^{-1}\,\mathrm{Mpc}) \leq 9$, the results are shown in Fig. 5. As in the ReBEL model, in both our N and C models the scalar field coupling makes the density profile steeper near and outside the boundary of the protovoids, and this effect is more prominent in early times (redshift 1.0, lower panels), which is not unexpected, because the fifth force helps the structure formation process to start (and low-density regions get evacuated) earlier, a fact which has also been confirmed by the observation that at early times the protovoids have notably lower density in the very inner regions in the coupled scalar field models than in ΛCDM. Note that the chameleon effect does play a role here, by making the protovoid density profiles in models C1 and C3 (for which $\alpha = 10^{-6}$ and the fifth force is most severely suppressed) indistinguishable from that of the L model; at later times (redshift 0.0, Fig. 5, upper right panel), however, the fifth force becomes less suppressed and the deviations from the L model gradually develop.

Fig. 6 displays the same results, but for the group of smaller (proto-)voids. Here we can see the similar trend as in Fig. 5, namely the scalar coupling produces steeper increase in the void density profile around the void edge. The effect is not as strong as for the large haloes, possibly because smaller voids form earlier and have been effectively evacuated even if the fifth force is not at play.

These results suggest that larger voids at earlier times could better reveal the influences of a possible scalar field coupling than smaller ones. Also, the strong-chameleon (C) and non-chameleon (N) models can be distinguished because for the former the void profile is essentially the same as the ΛCDM prediction at earlier times but starts to deviate later, while for the latter the deviation starts quite early. Note that the flatness of the inner density profile for voids in model L (Sheth & van de Weygaert 2004), which agrees with predictions of the simple spherical model (Gunn & Gott 1972; Lilje & Lahav 1991), is not changed much by the scalar field coupling.

Because of the limitation of resolution, we are unable to test the void profiles for very large and very small voids, which will be left for future work. Given the fact that large voids could be very different in size in different models, we expect that their density profiles could reveal more information about the physical models.

5 DISCUSSION AND CONCLUSION

Scalar-field-mediated long-range fifth forces have attracted much attention among cosmologists in recent years, and in most versions they come from a direct coupling between the matter species (usually dark matter only) and a cosmological scalar field. If they really exist, they might dramatically change the picture of cosmic structure formation, and alleviate or even solve some problems in the concordance ΛCDM model. On the other hand, the range and magnitude of the fifth force are often model dependent: on one extreme, represented by our N models, the effective potential $V_{\rm eff}(\varphi)$ is fairly flat so that the mass m_φ is light and almost the same everywhere; the fifth force then has a fixed ratio to gravity, which is equivalent to a rescaling of the gravitational constant. On the opposite extreme, like our C models, $V_{\rm eff}$ and thus the scalar field mass m_φ depends sensitively on the matter density in a way that m_φ could be very heavy in high-density regions, where the fifth force is severely suppressed and thus is negligible, but is quite light in the low-density regions, where the fifth force has a fixed ratio to gravity as in the N models. Furthermore, as emphasized by Li & Barrow (in preparation), the fifth force is often not the only impact the coupled scalar field could have on cosmology, nor even is it usually the most important one. In the N models, for example, the modification of the cosmic background expansion rate by the scalar coupling could be more influential in the course of structure formation Li & Barrow (in preparation).

The complexities indicate that the model-independent studies of the coupled scalar field might fail to appropriately account for the various effects due to the scalar field coupling (see Section 2 for a description). So in this paper, we have studied the formations

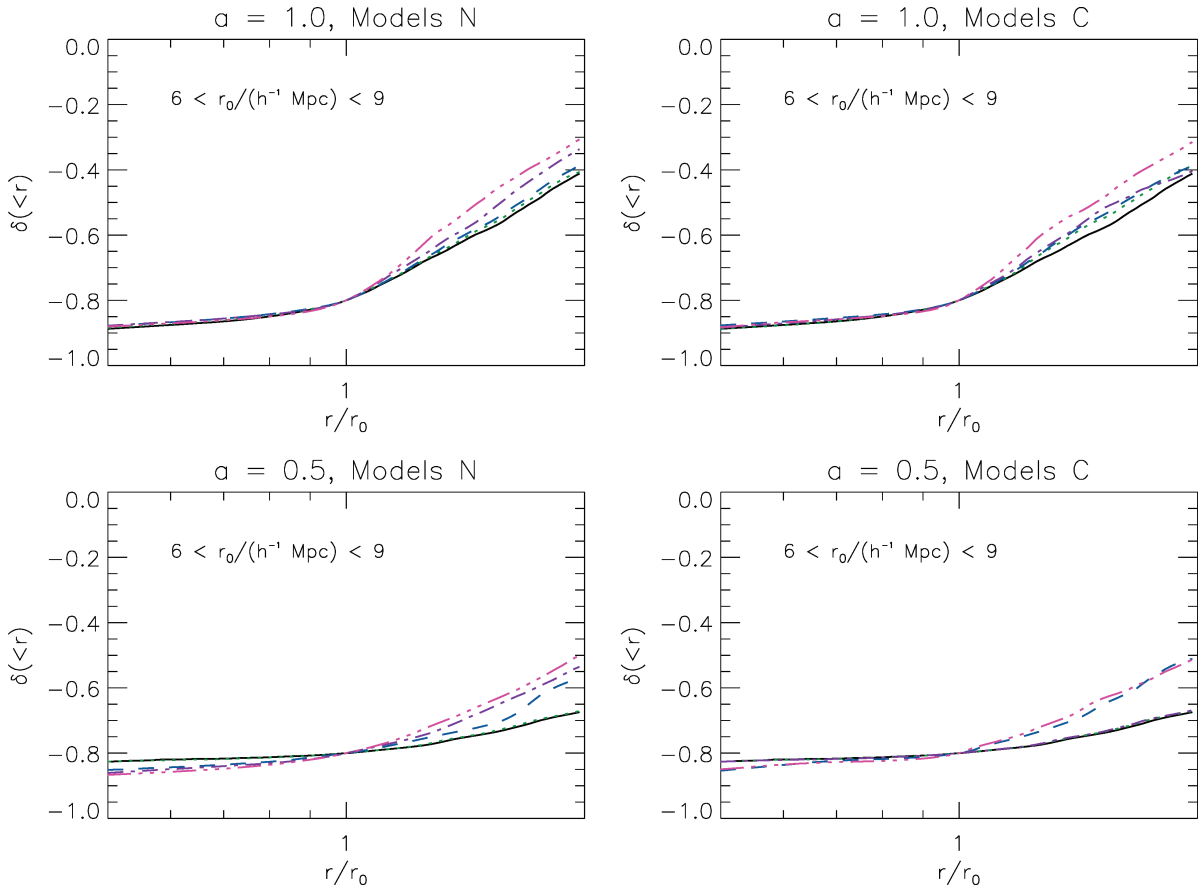

Figure 5. The density profiles of the protovoids whose radii fall in the range $6 \leq r_0/(h^{-1}\,\mathrm{Mpc}) \leq 9$. Upper left panel: Results at redshift 0 for the non-chameleon models N1 (green dotted curve), N2 (blue dashed curve), N3 (purple dot–dashed curve) and N4 (pink dot-dot-dot-dashed curve) in comparison to model L (black solid curve). Upper right panel: The same, but the green dotted, blue dashed, purple dot–dashed and pink dot-dot-dot-dashed curves now stand for model C1, C2, C3 and C4, respectively. Lower left panel: The same as the upper left panel but for redshift 1. Lower right panel: The same as the upper right panel, but for redshift 1. In all panels the horizontal axis is the distance from the protovoid centre, r, in the unit of the radius of the protovoids, r_0; the vertical axis is the dimensionless density contrast.

and properties of voids in the L, N and C models in parallel, and compared their predictions. Voids are the largest objects in the Universe which are produced during the course of structure formation, and fill the vast majority of the space. The importance of their properties in understanding the underlying cosmological scenario and global cosmological parameters has been emphasized by many authors. Recently, it has been claimed that a long-range fifth force could evacuate the space more efficiently and thus produce more voids than ΛCDM (Hellwing & Juszkiewicz 2009; Keselman et al. 2010). Those studies concentrate on the ReBEL model, where only a Yukawa-type fifth force is considered; because of the reason mentioned above, here we take into account all the main effects due to a scalar field coupling (which is arguably the most natural cause of a fifth force), consider two qualitatively different types of models and make a more detailed analysis of their effects on void properties by revising the void-finding algorithm.

Our Fig. 2 shows that in the coupled scalar field models matter is more concentrated in some regions, leaving the remaining space more evacuated, in line with expectations. Here we note that the N and C models behave differently: for the former, the fifth force is never suppressed, and the migration of matter from low-density regions to high-density regions starts earlier, thanks to it; for the latter, the chameleon effect suppresses the fifth force at the early times, the effect of which in boosting the clustering of matter has only become significant recently (after redshift 1). In both models, a larger portion of space is underdense today than in the L model.

We apply our void-finding algorithm to the N and C models, and find that both models predict a bigger number of larger voids than the L model does (Fig. 3). Once again, the N and C models behave quite differently, in particular at early times: by redshift 1.0 the N4 model produces several times more voids than the L model (and also the biggest voids are several times bigger), while the C models are only slightly different from the L model, though the fifth force in them, if unsuppressed, is much stronger than in the N models. The result seems to be contradictory to the expectation that in the void regions the fifth force gets less suppressed and therefore we should have seen a greater difference from the L model. The reason is as follows: first, the scalar field equation of motion is dynamical and the solution in the void regions depends on the overall environment in the simulation box, so it is untrue that the fifth force in void regions is unsuppressed; secondly, the formation rate of voids is more dependent on how fast high-density regions could pull matter out of them, but as the fifth force is suppressed this pull is not much stronger than in the L model.

It is worth noting that the difference between the void volume functions in N and L models is bigger at earlier times (Fig. 3), because at later times most potential void regions have already been developed: since there are not many more new voids yet to be

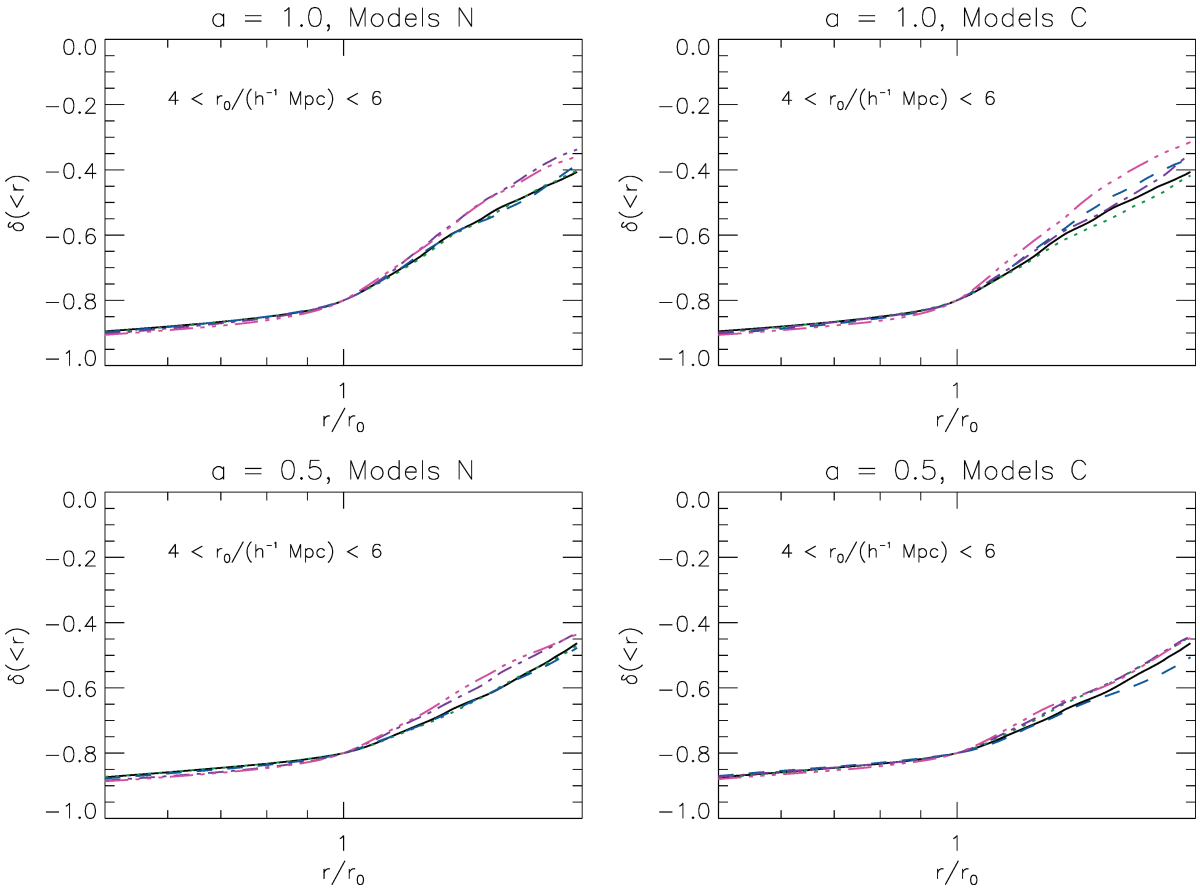

Figure 6. The same as Fig. 5, but for protovoids whose radii fall into the interval $4 \leq r_0/(h^{-1}\,\mathrm{Mpc}) \leq 6$.

produced in the N models, the L model gradually catches up. For the C models, the trend is quite opposite, and more voids are produced recently than in the L model, because finally the fifth force is freed and starts to take effect.

We also show in Fig. 4 the fraction of space which is filled by voids exceeding a certain threshold in volume. Here the qualitative features could be explained by the same argument used for Fig. 3, and what is more impressive is the quantitative result it illustrates. For example, at redshift 1.0 the N4 model, which is the most extreme in the N models, predicts almost four times as much space filled by voids larger than $35\,h^{-3}\,\mathrm{Mpc}^3$ as does the L model. Even at present the number is almost 2 (the same also applies to the C models). Voids prove to be a promising tool to constrain the scalar field couplings.

Finally, we have studied the density profiles of the voids (Figs 5 and 6). We find that in general the voids in the coupled scalar field models are featured by a sharper transition from low density to high density around their edges, similar to the result for the ReBEL model (Keselman et al. 2010). At earlier times the large voids in coupled scalar field models also have lower overdensities in the inner part due to the more effective evacuation of the region.

Due to the limitation of the simulation box and resolution, we have not studied other interesting void properties such as the haloes in voids. And because we have only dark matter in the simulations, we have not touched the formations and properties of the void galaxies. These shall be left to future works. The existing results, however, already indicate that the void properties could be largely influenced by a coupled scalar field, being it chameleon or not, and therefore voids could provide a useful tool to study and constrain such alternative scenarios for structure formation.

ACKNOWLEDGMENTS

The simulations and processing of data for this work were performed on the SARA supercomputer in the Netherlands, under the HPC-EUROPA project, with the support of the European Community Research Infrastructure Action under the FP8 'Structuring the European Research Area' programme, using a modified version of the publicly available MLAPM code (Knebe, Green & Binney 2001). The author thanks Rien van de Weygaert for detailed comments which helped to greatly improve the paper, and Lin Jia for helpful discussions and aid in the implementation of the void-finding algorithm. The author is supported by the Research Fellowship in Applied Mathematics at Queens' College, University of Cambridge, and the Science and Technology Facility Council (STFC) of the United Kingdom.

REFERENCES

Amendola L., 2000, Phys. Rev. D, 62, 043511
Armendariz-Picon C., Mokhanov V., Steinhardt P. J., 2000, Phys. Rev. Lett., 85, 854438
Baldi M., Pettorino V., Robbers G., Springel V., 2010, MNRAS, 403, 1684
Benson A. J., Hoyle F., Torres F., Vogeley M. S., 2003, MNRAS, 340, 160
Blumenthal G. R., Nicolaci da Costa L., Goldwirth D. S., Lecar M., Piran T., 1992, ApJ, 388, 234
Brans C. H., Dicke R. H., 1961, Phys. Rev., 124, 925

Brax P., van de Bruck C., Davis A. C., Shaw D. J., 2010, Phys. Rev. D, 82, 063519
Brunino R., Tsujillo R., Pearce F. R., Thomas P. A., 2007, MNRAS, 375, 184
Carroll S. M., De Felice A., Duvvuri V., Easson D. A., Trodden M., Turner M. S., 2005, Phys. Rev. D, 71, 063513
Colberg J. M., Sheth R. K., Diaferio A., Gao L., Yoshida N., 2005, MNRAS, 360, 216
Colberg J. M. et al., 2008, MNRAS, 387, 933
Copeland E., Sami M., Tsujikawa S., 2006, Int. J. Modern Phys. D, 15, 1753
Dubinski J., Da Costa L. N., Goldwirth D. S., Lecar M., Piran T., 1993, ApJ, 292, 371
Farrar G. R., Rosen R. A., 2007, Phys. Rev. Lett., 98, 171302
Foster C., Nelson L. A., 2009, ApJ, 699, 1252
Gunn J. E., Gott J. R., 1972, ApJ, 176, 1
Hellwing W. A., Juszkiewicz R., 2009, Phys. Rev. D, 80, 083522
Hoyle F., Vogeley M. S., 2002, ApJ, 566, 641
Hu W., Sawicki I., 2007, Phys. Rev. D, 76, 064004
Kesden M., Kamionkowski M., 2006, Phys. Rev. D, 74, 083007
Keselman J. A., Nusser A., Peebles P. J. E., 2009, Phys. Rev. D, 80, 063517
Keselman J. A., Nusser A., Peebles P. J. E., 2010, Phys. Rev. D, 81, 063521
Khoury J., Weltman A., 2004, Phys. Rev. D, 69, 044026
Knebe A., Green A., Binney J., 2001, MNRAS, 325, 845
Li B., Barrow J. D., 2007, Phys. Rev. D, 75, 084010
Li B., Barrow J. D., 2010a, Phys. Rev. D, in press (arXiv:1005.4231)
Li B., Barrow J. D., 2010b, preprint (arXiv:1010.3748)
Li B., Zhao H., 2009, Phys. Rev. D, 80, 044027
Li B., Zhao H., 2010, Phys. Rev. D, 81, 104047
Li B., Mota D. F., Barrow J. D., 2010a, preprint (arXiv:1009.1396)
Li B., Mota D. F., Barrow J. D., 2010b, preprint (arXiv:1009.1400)
Lilje P. B., Lahav O., 1991, ApJ, 374, 29
Maccio A. V., Quercellini C., Mainini R., Amendola L., Bonometto S. A., 2004, Phys. Rev. D, 69, 123516
Mo H. J., White S. D. M., 1996, MNRAS, 282, 347
Mota D. F., Shaw D. J., 2007, Phys. Rev. D, 75, 063501
Neyrinck M. C., 2008, MNRAS, 386, 2101
Nusser A., Gubser S. S., Peebles P. J. E., 2005, Phys. Rev. D, 71, 083505
Patiri S. G., Prada F., Holtzman J., Klypin A., Betancort-Rijo J., 2006, MNRAS, 372, 1710
Peebles P. J. E., 2001, ApJ, 557, 495
Perrotta F., Baccigalupi C., 1999, Phys. Rev. D, 61, 023507
Platen E., van de Weygaert R., Jones B. J. T., 2007, MNRAS, 380, 551
Plionis M., Basilakos S., 2002, MNRAS, 330, 399
Schaap W. E., van de Weygaert R., 2000, A&A, 363, L29
Shandarin S. F., Feldman H. A., Heitmann K., Habib S., 2006, MNRAS, 367, 1629
Sheth R. K., Tormen G., 2002, MNRAS, 329, 61
Sheth R. K., van de Weygaert R., 2004, MNRAS, 350, 517
Tinker J. L., Conroy C., 2009, ApJ, 691, 633
van de Weygaert R., Platen E., 2009, Modern Phys. Lett. A, 17, 21
van de Weygaert R., van Kampen E., 1993, MNRAS, 263, 481
Vollick D. N., 2003, Phys. Rev. D, 68, 063510
Wang L., Caldwell R. R., Ostriker J. P., Steinhardt P. J., 2000, ApJ, 530, 17
Zhao H., Maccio A. V., Li B., Hoekstra H., Feix M., 2010, ApJ, 712, L179

This paper has been typeset from a TEX/LATEX file prepared by the author.